Biosensors and Bioelectronics 123 (2019) 251–259

Contents lists available at ScienceDirect

Biosensors and Bioelectronics

journal homepage: www.elsevier.com/locate/bios

Fluorescence Interference Contrast-enabled structures improve the microarrays performance

S. Dobroiu[a,b,1], F.C.M.J.M. van Delft[c,d,1], J. Aveyard-Hanson[a], Prasad Shetty[a], D.V. Nicolau[a,b,*]

[a] Department of Electrical Engineering & Electronics, University of Liverpool, L69 3GJ, United Kingdom
[b] Department of Bioengineering, McGill University, Montreal, Quebec H3A 0C3, Canada
[c] Philips Research (MiPlaza), Philips Innovation Services, 5656 AE, Eindhoven, The Netherlands
[d] Molecular Sense Ltd., Liverpool L36 8HT, United Kingdom

ARTICLE INFO

Keywords:
Fluorescence Interference Contrast
Microarray
Signal/noise

ABSTRACT

Continuous improvements of the fluorescence-based sensitivity and specificity, required for high throughput screening, diagnostics, and molecular biology studies, are usually addressed by better readout systems, or better reporting elements. However, while Fluorescence Interference Contrast (FLIC), which modulates the fluorescence by materials-based parameters, has been used for decades to measure biomolecular interactions at nanometer-precision, e.g., for the study of molecular motors and membrane processes, it has been seldom used for high throughput or diagnostic microdevices. Moreover, the amplification of both the fluorescence signal, modulated by vertically-nano-calibrated structures, and the signal/background, modulated by laterally-micro-calibrated structures, has not been explored. To address this synergy, structures comprising optically transparent silicon oxide, tens of micrometers-wide and with thicknesses in the low hundreds of nanometers, which are able to promote the formation of standing waves if patterned on a reflective material, have been designed, fabricated and tested, for the use in DNA- and protein arrays. The light emitted by a fluorophore placed on top of the structures and reflected by a bottom mirror surface, e.g., silicon, platinum, is physically constrained to a region defined lithographically, both vertically and laterally, i.e., micro-pillars and –wells, resulting in an accurate identification and quantification of fluorescence. The signal/noise ratio on micro-/nano-structured substrates is comparable to that measured on planar substrates, but the physical confinement of the microarray spots results in a considerable increase of the intra-feature uniformity.

1. Introduction

Microarrays offer the advantage of a highly parallel, unsupervised identification and quantification of bio-molecular recognition events (Müller, 2005), but this rather straightforward high throughput analysis comes at the cost of having to process large amounts of data associated with the quantification of fluorescence signals of geometric patterns – the microarray spots.

For a given system of delivering the liquid samples, the quality of the printed features is the result of the interplay between processes taking place at the interface between a solid, liquid and gaseous phase: wetting, spreading, evaporation dynamics and transport phenomenon (McHale, 2007). For instance, the liquid transfer from a split pin to a surface is a result of cohesive and adhesive forces (Wu et al., 2012); and the intra-spot fluorescence distribution is a result of both droplet evaporation and contact line pinning (Deegan et al., 1997; Dugas et al., 2005; Hu and Larson, 2006; Moran-Mirabal et al., 2007). Further, the morphology of the printed features affects heavily the outcome of the detection and quantification process (Rickman et al., 2003; Wu et al., 2001) and, by extension, both the quality of the information extracted and the efficiency with which this is carried out, thus being an important source for variability and statistical uncertainty in microarray technology (Schuchhardt, 2000).

Because the algorithms designed to perform this quantification use the geometrical parameters of a microarray spot, i.e., its shape (Jain, 2002), dimension, and position (Lehmussola et al., 2006), as inputs, their quality and reproducibility will translate in the quality and reproducibility of the microarray data. The criticality of the geometrical parameters of microarray spots resulted in a vast variety of processing conditions aiming to optimize the printed feature morphology (Dawson et al., 2005; Taylor et al., 2003), such as humidity and various additives, e.g., betaine (Diehl et al., 2001), betaine and DMSO (McQuain

* Corresponding author at: Department of Bioengineering, McGill University, Montreal, Quebec H3A 0C3, Canada.
E-mail address: dan.nicolau@mcgill.ca (D.V. Nicolau).
[1] Equal first authors.

https://doi.org/10.1016/j.bios.2018.09.009
Received 20 June 2018; Received in revised form 18 August 2018; Accepted 1 September 2018
Available online 07 September 2018
0956-5663/

et al., 2003), or denaturants, e.g., DMSO and formamide in the presence of detergents (Rickman et al., 2003). Alternatively, there are parallel efforts to address the often imperfect geometrical patterns of microarray spots by the development of various approaches to feature extraction (Bozinov and Rahnenfuhrer, 2002). It follows that a microarray substrate that imposes a predefined, precise shape, size, and position of the microarray spots will inherently improve the feature extraction process and thus improve the quality of microarray data.

The continuous improvement of fluorescence-based sensitivity and specificity of microarrays is usually the result of improvements of better readout systems, or better reporting elements, e.g., fluorophores, quantum dots, rather than surface-based technical solutions. However, micro/nano-structured surfaces, which modulate the florescence of the surface-immobilized biomolecules and cells, have been successfully exploited to quantify, with nanometer precision, biomolecular interactions. Indeed, Fluorescence Interference Contrast (FLIC), which uses optical interference to modulate the intensity of the signal of a fluorophore as a function of its distance to a mirroring basal substrate, has been used to study the interaction between cytoskeletal filaments and protein molecular motors (Dumont et al., 2013; Kerssemakers et al., 2006, 2009; Nitzsche et al., 2016; Persson et al., 2010), the interactions between membranes and various tethered biomolecules (Ajo-Franklin et al., 2005; Chung et al., 2009; Crane et al., 2005; Dabkowska et al., 2015; Ganesan and Boxer, 2009; Kaizuka and Groves, 2006; Parthasarathy and Groves, 2004a, 2004b) and processes in cells immobilized on surfaces (Braun and Fromherz, 1997; Gleixner and Fromherz, 2006; Iwanaga et al., 2001; Kiessling et al., 2000; Sorribas et al., 2001; Zeck and Fromherz, 2003). Despite this rather extensive work, FLIC-enabled micro/nano-structures have not been used in microarray technology.

To this end, the present contribution proposes the use of FLIC-enabled, finely-calibrated micro/nano-structured surfaces, which amplify the fluorescence resulting from biomolecular recognition events, as well as quenching the parasitic fluorescence background, thus improving the signal/noise ratio. These FLIC-enabled structures also provide precise geometrical patterns for microarray spots, thus increasing the uniformity of the spot fluorescence and therefore the quality and reproducibility of microarray data.

2. Methods and materials

2.1. Microarray substrates

The fabrication of FLIC-enabled structured surfaces used standard semiconductor manufacturing. Briefly, silicon wafers were used as received if silicon was the reflective material. Alternatively, a 100 nm platinum layer has been deposited, if chosen as reflective material, on the 10 nm titanium layer deposited on silicon wafer to improve the adhesion between Pt and Si. The fabrication of the reflective surfaces was followed by the deposition of silicon dioxide layers, as spacers, with thicknesses of 20, 40, 60, 80 and 100 nm. The SiO_2 spacer layers on all surfaces were patterned by optical lithography, followed by SiO_2-etching, to obtain rectangular FLIC-enabled structures with lateral dimensions of 1, 1.25, 1.5, 2, 3, or 5 μm (areas of 1, 1.5625, 2.25, 4, 9, and 25 μm^2). The fabrication process is presented in Fig. 1A (detailed fabrication protocols are presented in the Supplementary information section). The FLIC-enabled structures were characterized by optical, and by Atomic Force Microscopy (AFM, Fig. 1B).

Following the optimization of the geometry of the FLIC-enabled structures, another set of microarray substrates were fabricated with using the same procedures, but presenting both SiO_2 pillars, and wells, with optimum rectangular footprints (area: 25 μm^2). Negative control areas, on which no FLIC response is expected, comprising flat, non-processed areas (Control 1, withnative SiO_2), and positive control areas (Control 2, with SiO_2 layers with the same thickness as the adjacent optimized FLIC structures), on which FLIC response is expected were present on the same microarray surface. The surfaces in all stages of use were characterized by TOF-SIMS analysis.

Commercially available, high sensitivity substrates, i.e., Nexterion E and HiSens E epoxy coated slides, purchased from Schott AG (Mainz, Germany), were also used as controls.

2.2. Functionalization and biomolecular recognition

The functionalization of microarray substrates used either (3-aminopropyl)triethoxysilane (APTES), or (3-Glycidyloxypropyl)trimethoxysilane(GPTES).

APTES has been used for the initial calibration of the optimum geometry of the FLIC-enabled structures. Briefly, following the functionalization of the SiO_2 surface with amino groups, the differential fluorescence has been revealed via the reaction with NHS ester-derivatised fluorescent dye (DyLight 649). To demonstrate the viability of the FLIC-enabled surfaces for microarray-type applications, for oligonucleotides, and for proteins, respectively, the FLIC-enabled structures were further functionalized with the avian flu virus strand, or biotinylated, respectively, then the differential fluorescence signal was revealed by hybridization with Cy-5 labeled cDNA, or FITC-labeled streptavidin, respectively (Fig. 1C).

The GPTES-based procedure, which was thoroughly optimized (details in Supplementary information section), was used to quantify the performance of FLIC-enabled arrays, benchmarked against controls, and against high sensitivity microarray substrates. Briefly, the amino-functionalized FLIC-enabled structures and the controls were further functionalized with synthetic oligonucleotides with the probe with a sequence: 5′ CCTCAAAGAGAGAGAAGAAGAAA 3′, with a C6 amine modifier at the 5′ end; then these probe-functionalized surfaces were hybridized with the complementary target with a sequence: 5′ TTTCT TCTTCTCTCTCTTTGAGG 3′, with a Cy5 modification at the 5 end.

The printing of the capture probes was carried out in a manner consistent with the protocol recommended by Schott for their high sensitivity slides (Conzone and Redkar, 2004). The hybridization was carried out using solutions containing different target concentrations, from 1 to 3.2 × 10–11 μM. Post hybridization washes were carried out for 10 min as per the Schott protocol. After washing, the slides were dried in a gentle stream of nitrogen.

Full and detailed description of the protocols regarding the functionalization and subsequent hybridization of the microarray substrates is provided in Supplementary information.

2.3. Instrumentation

Optical fluorescence microscopy used a Zeiss Observer microscope equipped with a LSM 510 laser scanning confocal module. AFM imaging was carried out using a CP-II atomic force microscope (Veeco, USA) equipped with a large area scanner. Tapping mode scanning was employed using silicon probes attached to cantilevers with a typical force constant of 40 N/m and a typical resonance frequency of 300 kHz (Budget Sensors, Windsor Scientific, UK). The contact angle measurements used a Drop Shape Analysis System DSA 10 Mk2 (Kruss, Germany). Surface adsorbates decontamination was carried out in a Bioforce Nano UV-ozone chamber (Bioforce Nanosciences, USA). Finally, microarray spots were printed with a VP 478A Floating Pin Replicator using manual split pins with a capacity of 500 nL (V&P Scientific, San Diego, USA). Test substrates were imaged on a GenePix 4000B Microarray Scanner (Molecular Devices, USA).

2.4. Image analysis and quantification

The image analysis of all fluorescent samples used the laser scanning confocal microscope. Excitation was achieved using a 633 nm laser line and the emission was collected using a 650 nm long pass filter. The images, in their original format, were processed using the freely

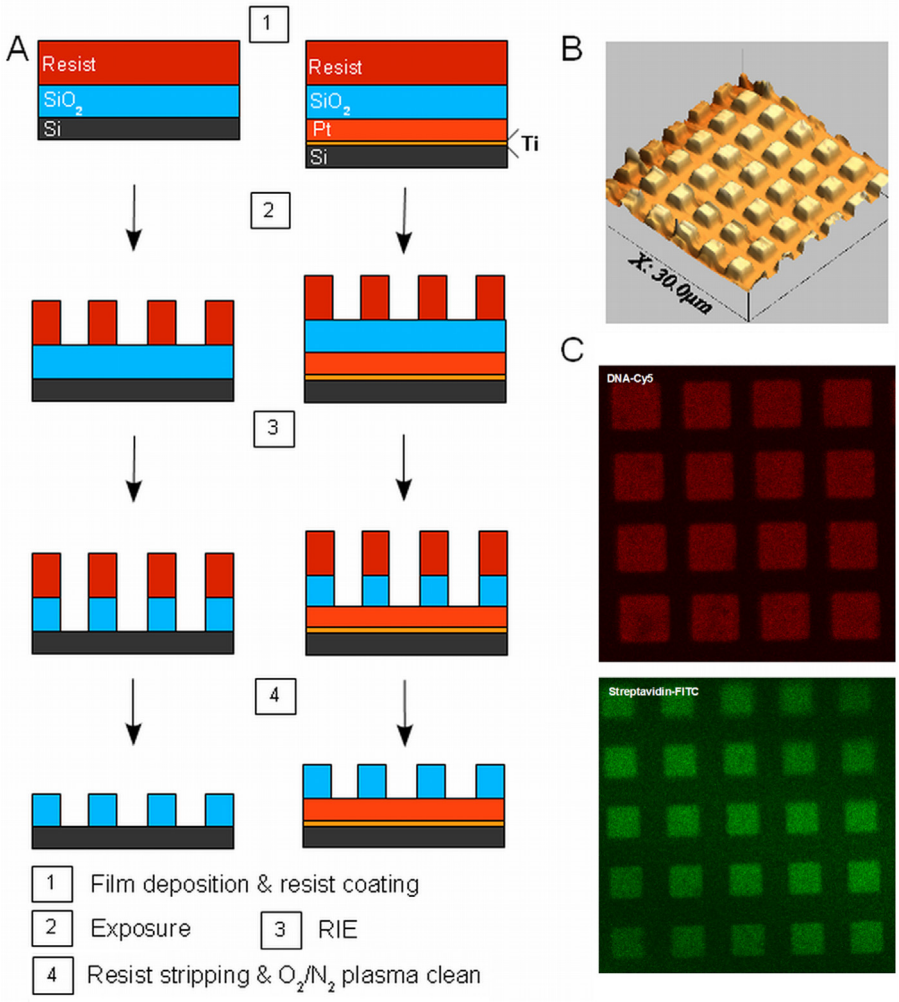

Fig. 1. Micro/nano-structured microarray surfaces. A. Fabrication process. Reactive Ion Etching (RIE) is required to etch vertically the structures. B. An (AFM) topography scan (the height of the pillars is exaggerated and the walls appear rounded due to the small vertical dimensions compared with the apex of the AFM tip). C. Cy-5 modified avian flu virus sequence (left) detected through hybridization and streptavidin-FITC (right) mounted on biotinylated micro/nano-structures.

available ImageJ package (Rasband 1997–2011) together with the Zeiss Laser Scanning Microscope (LSM) Reader and the LSM Toolbox plug-ins. The extracted parameters, i.e., surface area; signal mean, background mean and standard deviation and the integrated signal intensity were processed further using the commercially available software Origin (Origin Lab, Northampton, MA, USA). Full details regarding the image analysis and quantification are presented in Supplementary information.

3. Results and discussion

3.1. Optimization of the parameters of the micro-/nano-structured microarray substrates

3.1.1. Selection of materials

The well-developed mathematical formalism of the standing wave effect (Levinson, 2005) associated with FLIC (Brandstatter et al., 1988; Lambacher and Fromherz, 1996, 2002; Nakache et al., 1985), presented in detail in the Supplementary information section, would, in principle, make the selection of materials for the micro/nano-structured surfaces straightforward. Indeed, from the optics point of view, the amplification of the fluorescence signal requires the most transparent material for the spacer layer, and the most reflecting material for the mirroring surface. However, for the real FLIC-enabled structured surfaces additional issues need to be considered, as follows.

- First, the chosen materials for FLIC-enabled structures must be amenable to micro- and nanofabrication, preferable by classical semiconductor manufacturing techniques. Also, the adhesion between the spacer and the reflecting material must be excellent, or alternatively, intermediate layers should be made available, but these should not reduce the optical properties of the reflecting surface or the spacer layers.
- Second, if the standard electrode potential of the two materials in contact is too different, then the junction between them, e.g., surrounding the FLIC-enabled structures, in contact with the buffered fluid containing analytes, will operate as an electrolytic cell, further damaging the contact between the spacer and the reflector, and possibly changing the composition of the analyte fluids.
- Third, the interplay between the geometry of the structured surface, e.g., pillar, wells, and the surface tension of the reflecting and spacer materials, modulate the wettability at the micro, or even nano-scale (Kašpar et al., 2016), thus impacting on the final lateral distribution of microarray spots.
- Fourth, the selection of two materials could, in principle, offer the opportunity of using their different nature to improve the signal/background ratio. Indeed, gold, which has a high reflectivity, can be functionalized using thiol-based chemistry, to repel target biomolecules, e.g., proteins, while the SiO_2 spacer structures could be functionalized using a different chemistry to ensure a high concentration of probe biomolecules (Kašpar et al., 2016).

Considering the above, SiO_2, and Si or Pt, were chosen as the spacer, and reflecting material, respectively. Indeed, SiO_2 has very good transparency, i.e., above 90% for the visible spectrum. While Au has a very good reflectivity, and also offers very good alternative chemistry vs. the one to be used for silicon-based materials, it has to be avoided as reflecting material due to its poor adhesion to SiO_2, as well as large difference in standard electrode potential, in particular in low pH buffers (Bartolini et al., 2013). Conversely, Si has an inherently perfect adhesion to SiO_2 and reasonable reflectivity, i.e., 30–40% (Huen, 1979; Wu and Chiou, 1996a, 1996b). Finally, while Pt has a very good reflectivity, i.e., nearly 80% (Yu et al., 1968), it has a less-than perfect adhesion to SiO_2, requiring more careful fabrication protocols, e.g., slower deposition of layers. All materials are amenable to well-established semiconductor manufacturing protocols.

3.2. Optimization of the geometry of the FLIC-enabled micro/nano-structures

The theoretical description of the FLIC phenomenon (Brandstatter et al., 1988; Lambacher and Fromherz, 1996, 2002; Nakache et al., 1985) allows for an unambiguous prediction of the modulation of the signal of a fluorophore placed at the top of the FLIC structure by its height. Essentially, when a fluorophore is placed above a reflecting surface, its emitted light directed towards the basal surface is subject to interference upon reflection from the bottom mirror (the light initially directed away from the basal surface is not affected). Depending on the wavelength of the emitted light, the distance between the fluorophore and the mirror induces a relative amplification, or quenching, of the fluorescence signal. Full details of the theoretical background are presented in Supplementary information section, and the principle is presented in Fig. 2A. For instance, the fluorescence signal of the Cy5 fluorophore placed on a SiO_2 pillar (spacer) mounted on a Si surface (reflector) reaches a maximum at approximately 100 nm height of the pillar (Fernandez, 2009a), regardless of the reflectivity of the mirror surface. Conversely, a relative quenching of the fluorescence signal is obtained for distances between the fluorophore and the mirror surface around 200 nm. Finally, because FLIC phenomenon is recursive, i.e., the fluorescence maxima and minima appear, sequentially, with the increase of the distance between the fluorophore and the reflecting surface, various designs of the FLIC-enabled structures are possible. For instance, the pillars-based design (Fig. 2B top) will induce the relative amplification of the fluorescence on the top of the pillars, comparative with the neutral fluorescence from the fluorophores present on the basal surface (if this has the same chemical nature as the top of the pillars). Alternatively, a wells-based design (Fig. 2B bottom) will induce the amplification of fluorescence at the bottom of the wells, but also the quenching of fluorescence from the fluorophores placed on the approximately 200 nm-high pillars.

Although the fundamentals of FLIC phenomenon are largely established, there are many other parameters, e.g., imperfect reflection, non-normal light incidence, fluorophore molecular orientation, modulation of the actual emission by the molecular environment of the fluorophore, light polarization, variation of the optical properties of materials due to fabrication processes, etc., which impact on the actual optimum height of the spacer pillar. Consequently, experimental efforts to find the optimum vertical dimensions for the FLIC structures, taking those predicted by FLIC theory as guidelines, are fully warranted. Preliminary experiments revealed that many of the predictions of the FLIC theory hold. For instance the maximum fluorescence, for Cy-5-labeled molecules, is obtained for heights of the FLIC pillars of approximately

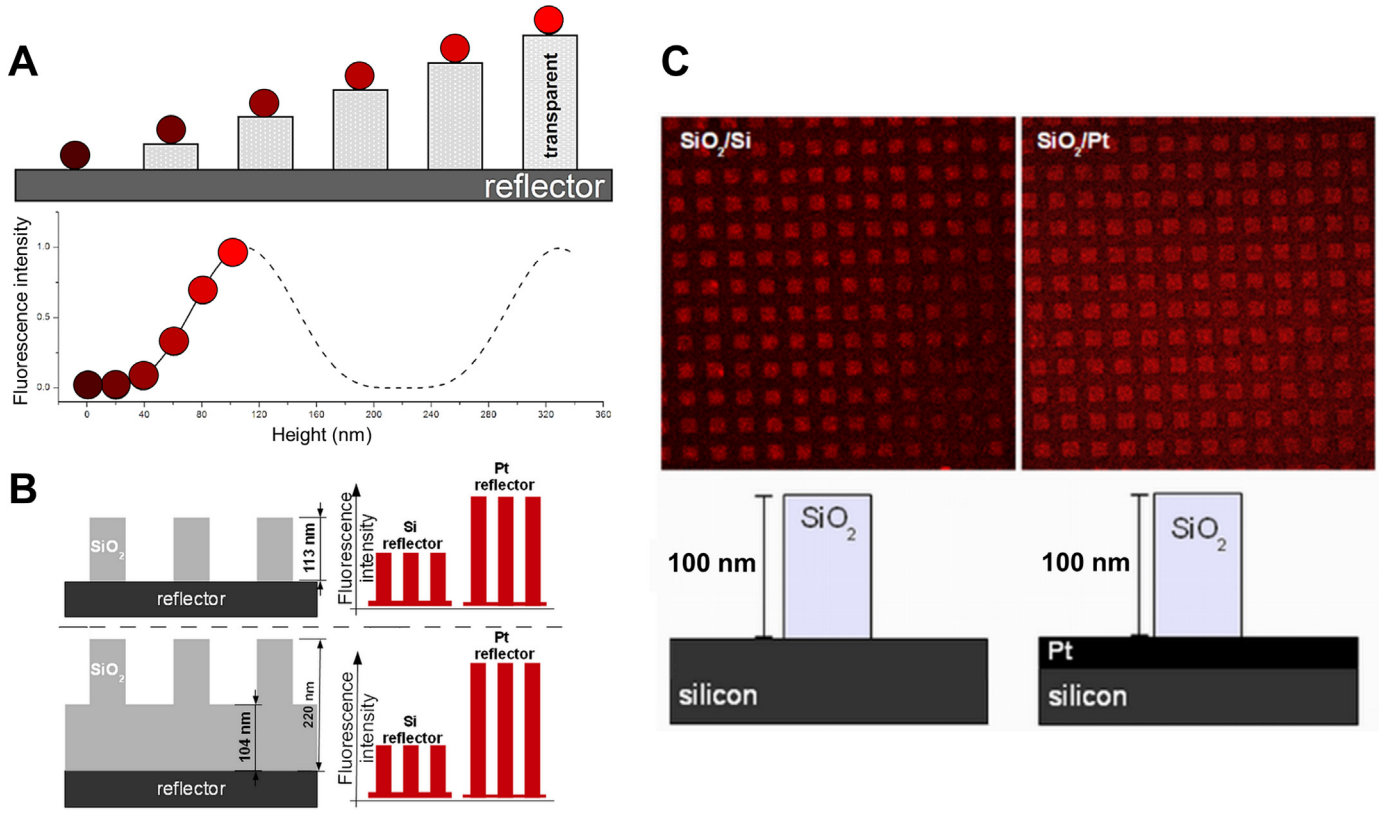

Fig. 2. Modulation of the fluorescence signal by the height of the microstructure. A. The emitted light from a fluorophore placed at a distance from a reflecting surface is, upon reflection, subject of optical interference, which results in its relative amplification, until a maximum uniquely determined by the wavelength of the light. After this maximum, the further increase of the distance between the fluorophore and the mirror surface will result in a quenching effect. B. The optimum design of the micro-pillars (top), and micro-wells (bottom), patterned on a Si, or Pt surface used as reflector (drawing not to scale). C. Detection of the avian flu virus on FLIC-enabled structures.

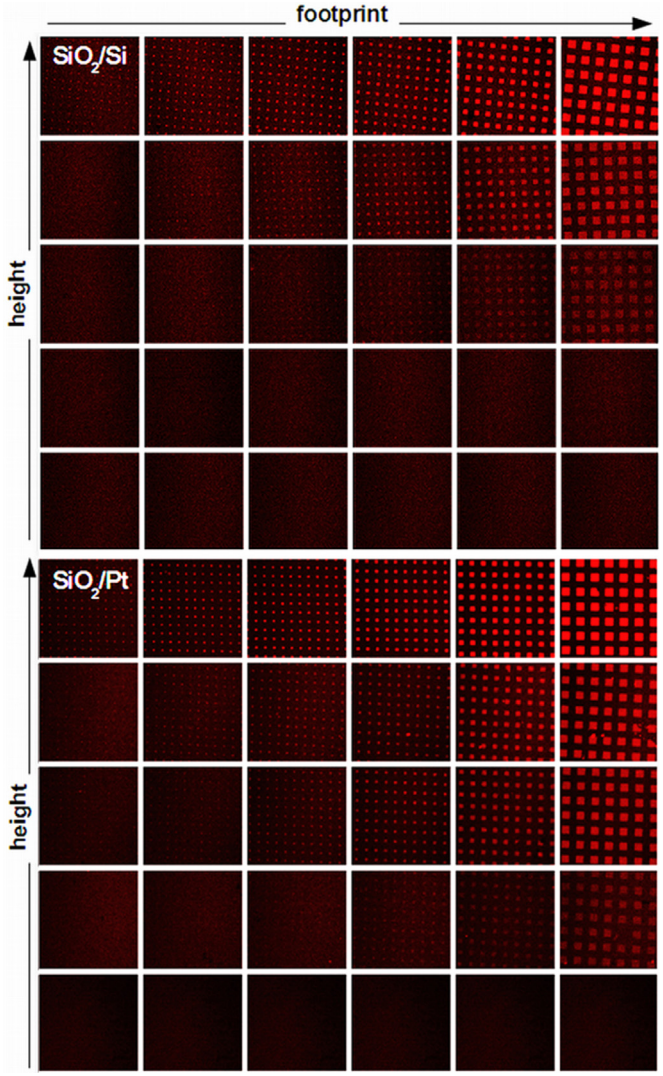

Fig. 3. Modulation of the fluorescence by the *width* of the micro-pillars. The effect of the height of the micro-terrace (increasing from bottom to top) and footprint (increasing from left to right) on the amplification of fluorescence for silicon oxide microstructures on silicon (top) and platinum (bottom).

100 nm, and conversely, the minimum fluorescent intensity is observed for distances between the fluorophore and the reflector around 200 nm (Fig. 2A). Also, the overall intensity of the fluorescence signal is considerably weaker on structures standing on Si than those on Pt, due to the considerable lower reflectivity of the former (scheme in Fig. 2B right; experimental validation in Fig. 2C). Finally, it was experimentally demonstrated that the region around 100 nm, being the first region in the FLIC amplification spectrum, could produce notable amplifications for several fluorophores with quite different emission wavelengths, e.g., Cy5 (670 nm), FITC (518 nm), as presented in Fig. 1 Cl (Supplementary information Fig. SI2).

The variation of the overall fluorescence signal/unit area with the *lateral* dimension of the FLIC structures is more difficult to control. Indeed, Fig. 3 presents the fluorescence signal on pillars with the optimum height for Cy5 fluorophore, i.e., 100 nm, but for areas where the FLIC-enabled structures have lateral dimensions starting from 1 to 5 μm. A brief inspection of the variation of fluorescence signal versus the area of the FLIC-enabled structures shows that the fluorescent images with the best contrast, be that on Si, or Pt, are obtained for structures with the largest area. Furthermore, the quantification of the fluorescence signal/unit area (Supplementary information Fig. SI4) demonstrates that FLIC-enabled structures with a footprint of 25 μm^2 are capable to deliver an amplification of up to 4 × , and 3 × , for Pt-, and Si-based substrates, respectively, but only 2.5 × , and 1.5 × , for the same surfaces footprints of 1 μm^2. This reduced amplification is remarkable, in particular as the top area of the FLIC structures per unit area, e.g., 100 × 100 μm, is identical for all footprints considered. The amplification effect reaches a plateau around 10–25 μm^2 (Supplementary information Fig. SI5). Several explanations are available, some of the most probable as follows. First, the roughness of the vertical walls, which increases for smaller features due to the more difficult lithographic reproduction, are likely to have a deleterious, light-absorbing effect on the light reflected from the mirror surface. Moreover; these optical edge effects amplify for smaller features, as the ratio of the area of vertical walls versus the pillar footprint is considerably larger for small features, e.g., 4:1 for a 1 × 1 μm pillar versus 20:25 for a 5 × 5 μm one. Second, an optical absorbance effect could be the result of the parasitic lateral reflections on the non-vertical walls, relatively more prevalent for smaller features. Third, smaller pillars may induce deleterious interference effects in structures with dimensions closer to the wavelength of the light passing by. Whatever the explanations for the decrease in the amplification of fluorescence by the decrease of the area of the FLIC-enabled substrates, further experiments quantifying their performance used structures with the optimum 25 μm^2 area.

3.3. Performance of the micro-/nano-structured microarray substrates

3.3.1. Signal/noise ratio

One of the main performance parameters of a microarray image is its Signal/Noise Ratio (SNR). Classically, SNR definition assumes that the 'true' *signal* comes from the biomolecular recognition between the probe immobilized on the surface and the fluorescently-labeled target in the solution in contact with the surface. Then *noise* is the result of the florescence of the target molecules which did not interact with the probe molecules, but have been immobilized on the surface via non-specific adsorption. In reality, the noise is also often the result of the fluorescence not related to the target, e.g., the background fluorescence of the surface. Whatever the components of the noise, a high SNR allows the user to amplify the power of the excitation light, and thus boost the signal, and consequently detect lower concentrations of the target analyte. Conversely, a low SNR will make it the quantification of the signal difficult, or unreliable, possibly even for high concentrations of the target.

While interference effects are used (Redkar et al., 2006; Schultz et al., 2011) for the overall amplification of the florescence on highly-sensitive, albeit flat, microarray substrates, such as Nexterion HiSens E, the *patterned* FLIC-enabled structures (Fernandez, 2009b) offer two additional opportunities for SNR maximization. First, the distinctly different materials of the elevated FLIC-enabled structures, and the surrounding reflecting surfaces, allow the deployment of very different chemistries, optimized for the efficient immobilization of the probe molecules on the top of FLIC structures, and for specifically repelling target molecules outside the FLIC-enabled areas. Second, FLIC can be used not only for the amplification of the signal on FLIC-enabled structures, but also, separately, for the extinguishing of the parasitic fluorescence outside the FLIC areas.

Fig. 4 presents the variation of the intensity and contrast of the microarray spots deposited on high sensitivity, commercially available substrates (Nexterion E and Nexterion HiSens E), and on FLIC-enabled structured surfaces, both as pillars and as wells, and on using Si, or Pt, as reflectors, modulated by the concentration of the target in the analyte solution. While it is evident that the intensity of the fluorescence signal is stronger on the high sensitivity, commercial substrates (in particular Nexterion HiSens E), the Pt-based, pillar architecture of the FLIC-enabled structures can also detect the lowest concentration of the target. In this context, it should be noted, however, that only half of the total area of the FLIC-enabled structures is actually available for

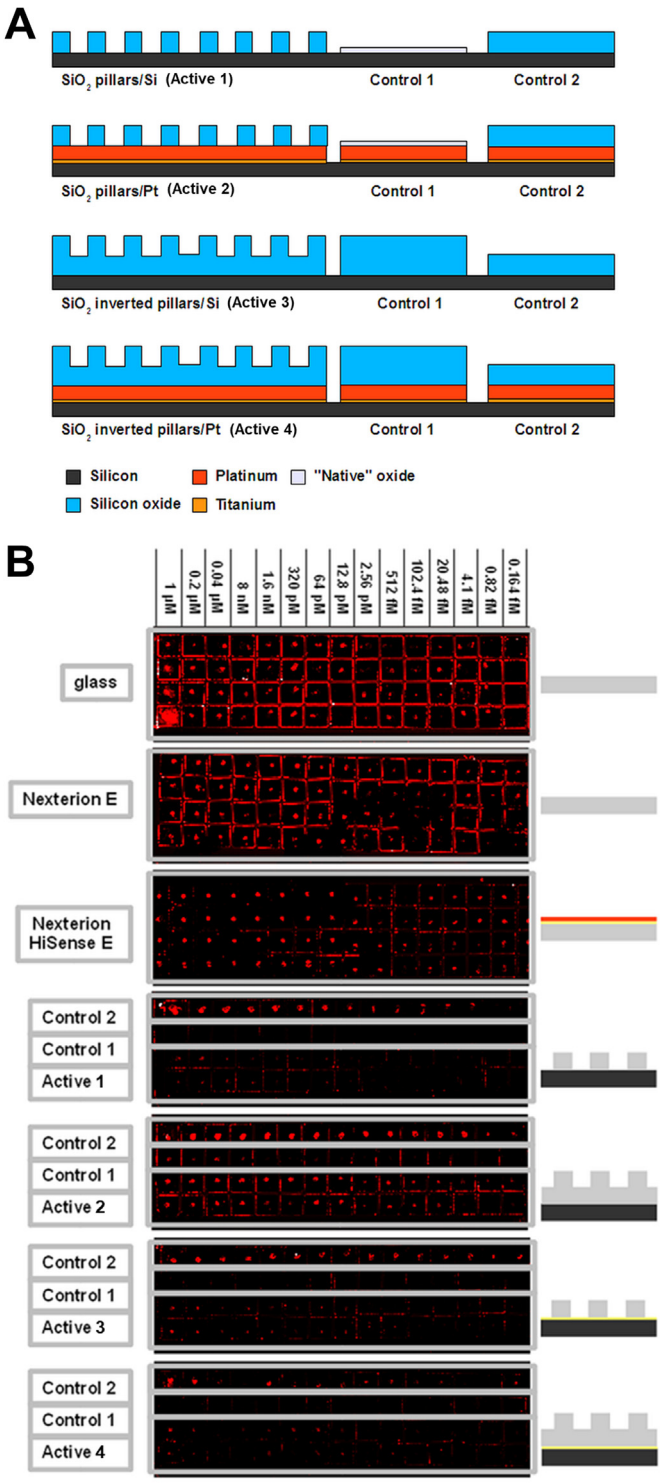

Fig. 4. A. Schematic cross-section view through the four FLIC-enabled substrates (active areas, containing micro-pillars and micro-wells, respectively), negative control surface (Control 1, comprising flat, non-processed, native SiO_2 areas), and a positive control surface (Control 2, comprising flat SiO_2 layers with the same thickness as the adjacent optimized FLIC structures). B. Fluorescence micrographs of entire substrates after hybridization. From top to bottom, these substrates are plain glass, Nexterion E, Nexterion HiSens E, micro-pillars/ on Si, micro-wells/on Si, micro-pillars/on Pt and micro-wells/on Pt (a descriptive sketch of each substrate type is shown on the right side of the image).

fluorescence signal, the rest being taken by the spaces between pillars (or wells), and consequently the sensitivity of detection relative to the detection area is considerably higher.

Despite the lower overall signal, to be improved by further optimization, the laterally-defined geometry of the FLIC-enabled structures offers important benefits for signal quantification. The procedure used for data extraction in microarray technology is based on the Otsu thresholding algorithm (Rueda and Rezaeian, 2011). For FLIC-enabled substrates, the same type of thresholding was initially applied to ensure non-biased identification the area where the sub-spots are, followed by a selection comprising a 3 × 3 array of 6 × 6 pixels superimposed on a set of nine sub-spots, then followed by the automated determination of the area where the sub-spots (FLIC pillars or wells) were located (Fig. SI6 in Supplementary information section). Further, the non-square sub-spots, prevalent at the borders of the spot, were excluded, on the basis of the underlying design concept of the substrates as sets of only rectangular, 5 × 5 µm 'pixels' (Fig. SI7 in Supplementary information section). The statistical relevance was easily achieved, as FLIC-enabled structured surfaces present 270 pixels, whereas the number of pixels per spot deemed statistically sufficient in the microarray literature ranges between a minimum of 25 (Dufva, 2005) or, generally, a pixel size of a tenth of the spot diameter (Schena, 2003). This spatially-assisted quantification of the fluorescence signal on FLIC-enabled structured surfaces, which is free of the uncertainties related to the finding the spot boundaries, delivered a better than expected SNR (Fig. 5), in particular for higher concentrations of the target.

The florescence signals on both microstructured and positive control surfaces (top and bottom, respectively, in the right panel in Fig. 5) are approximately one order of magnitude higher than that of the background on microstructured surfaces (middle graph in the right panel in Fig. 5). However, as a result of the more even spatial distribution of the fluorescence intensity on microstructured surfaces than on the flat positive control (see also Fig. 6, right panel), and thus a better integration of the fluorescence signal, a clear correlation between the fluorescence signal on microstructured surfaces (and of the background) and the target concentration can be inferred, as opposed to the more scattered data resulted from the deposition on flat control surfaces.

3.4. Intra-spot signal uniformity

The measures used to quantify the data resulting from each spot (whether mean, median, mode, etc.) do not offer any information about the spatial distribution of the fluorescence intensity inside the spot, but non-uniform spots result in the degradation of the quality of, and the confidence in the data. A simple and useful spot metric that can provide a general uniformity estimate is the Relative Standard Deviation (RSD), given by the ratio between the standard deviation and the mean spot intensity (Moran-Mirabal et al., 2007). Using this figure of merit, the performance of the FLIC-enabled substrate appears to be superior to those of flat, non-structured areas, i.e. the positive control region (Fig. 6).

While the elevated fluorescence distribution is readily apparent when compared to the corresponding flat control area, there is a set of benefits arising from the composite spot structure. One such advantage, briefly discussed above, is the introduction of a structuring element that can objectively deliver a rejection criterion. Thus, a geometric threshold where sub-spots that do not take the shape imposed by the substrate, square in this case, can be disregarded without compromising the whole data-set, i.e., the array of sub-spots comprising the spot. Another important point is the limitations imposed by the reflector material. To our best knowledge, the only commercial fluorescence enhancement slide available (Redkar et al., 2006; Schultz et al., 2011) is based on a dielectric stack coating. However, it was shown that the performance of such a slide can be matched, or surpassed by using a single silicon oxide layer and a highly reflective basal layer (Marino et al., 2008). The authors have assigned the improved performance to

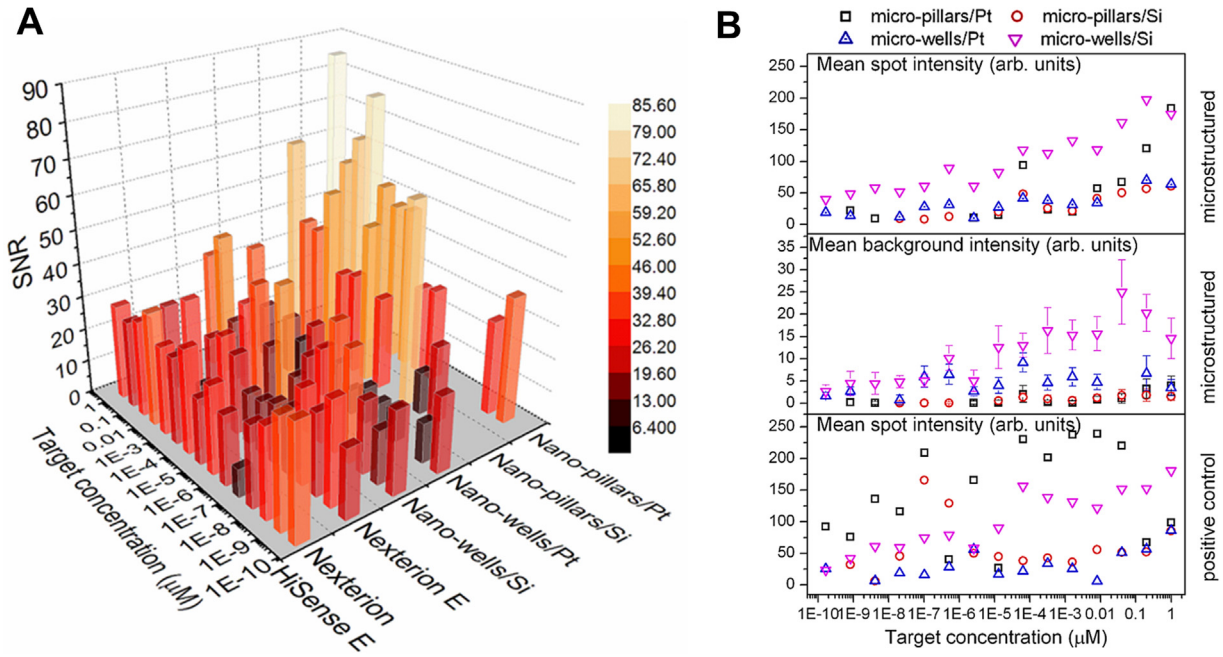

Fig. 5. A. Comparison of the contrast of the fluorescence signal on the spot, quantified by the Signal/Noise Ratio (SNR) (vertical axis), for two commercial substrates (Nexterion HiSense E and Nexterion E), and four types of FLIC-enabled structures, i.e., pillars and wells, on Si, and Pt, respectively (right horizontal axis), versus the target concentration (left horizontal axis). B The variation of the individual components of SNR versus target concentration: top mean spot fluorescence intensity on microstructured surfaces; middle: mean background fluorescence intensity on microstructured surfaces; bottom: mean fluorescence intensity of the spots printed on positive controls).

the immunity to changes in refractive index taking place in the immediate vicinity of the coating, as opposed to the dielectric stack whose fluorescence enhancement properties are affected by the optical properties of the media immediately outside the stack. This is made possible in the micro-well architecture where a silicon oxide insulation layer protects the reflector surface and thus a whole range of materials, e.g. aluminum, silver, which might otherwise not be optimal for operation in fluid aqueous environment.

4. Conclusion

The design and fabrication of Fluorescence Interference Contrast-enabled micro/nano-structured surfaces have been optimized with regard to the amplification of the fluorescence signal, the signal/noise ratio, and signal uniformity in the microarray spots. The enhancement of fluorescence by FLIC-enabled structures, with an optimum height of 100 nm, and an optimum footprint of 5 × 5 μm, was demonstrated both via oligonucleotide hybridization and streptavidin attachment on

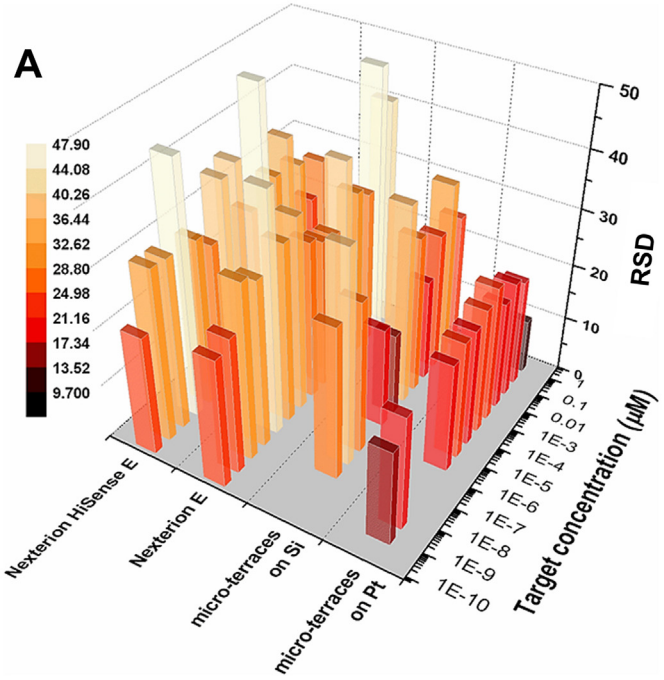

Fig. 6. A. Comparison of the uniformity of the fluorescence signal on the spot, quantified by the Relative Standard Deviation (RSD) (vertical axis), for two commercial substrates (Nexterion HiSense E and Nexterion E), and two types of micro/nano terraces, on Si, and Pt, respectively; left horizontal axis) versus the target concentration (right horizontal axis). B. False color representation of the spatial distribution of the fluorescence signal on a spot printed on a commercially substrate (top) and printed on structured substrates (pillars, bottom).

biotinylated structures. Using this optimum design, the performance of four FLIC-enabled surfaces, comprising pillars, or wells; on Si, or Pt, respectively, was benchmarked against that of commercial microarray substrates. While the FLIC-enabled substrates offer a comparable, but lower fluorescence signal than that of high sensitivity commercial microarray slides, the spatial distribution of the fluorescence intensity is more even on FLIC-enabled substrates than on flat surfaces. Furthermore, the embedded information regarding the distribution, shape, and size of the FLIC 'pixels' allows for a better classification of the signal, and the background noise, respectively, resulting in a signal/noise ratio equivalent to the high end microarray substrates. Because the optimum design and choice of materials is a function of the fluorophores, and the buffer used, respectively, further work would be required to tailor the FLIC-enabled structures according to specific applications. It is also envisaged that the use of micro-structured substrates can improve the automated detection process and thus the reliability of the resulting data for microarray applications.

Acknowledgements

The research received funding from the European Union Seventh Framework Programme (FP7/2007-2013) under grant agreement n° [214538] project Bio-Inspired Self-assembled Nano-Enabled Surfaces (BISNES); and Natural Sciences and Engineering Research Council (NSERC) of Canada under a Discovery Grant (RGPIN-2016-05019). The authors thank Drs. Jeroen van Zijl, Jaap Snijder, and Eric van den Heuvel from Philips Research for contributing to the fabrication of the FLIC-enabled structures, Jurgen van Berkum from Philips Research for TOF-SIMS analysis.

Authors' contribution

SD and DVN designed the experiments. FvD fabricated the micro/nano-structures. SD performed the work regarding microarray performance. JA-H contributed to functionalization and hybridization work. PS contributed to data analysis. DVN directed the research.

Appendix A. Supporting information

Supplementary data associated with this article can be found in the online version at doi:10.1016/j.bios.2018.09.009.

References

Ajo-Franklin, C.M., Yoshina-Ishii, C., Boxer, S.G., 2005. Probing the structure of supported membranes and tethered oligonucleotides by fluorescence interference contrast microscopy. Langmuir 21 (11), 4976–4983.
Bartolini, M., Naldi, M., Nicolau, D.V., Van Delft, F.C.M.J.M., Van Zijl, J., Snijder, J., Van Den Heuvel, E.F.C., Naburgh, E.P., Calonghi, N., Andrisano, V., 2013. Fluorescence biosensing micropatterned surfaces based on immobilized human acetylcholinesterase. Anal. Bioanal. Chem. 405 (2–3), 795–804.
Bozinov, D., Rahnenfuhrer, J., 2002. Unsupervised technique for robust target separation and analysis of DNA microarray spots through adaptive pixel clustering. Bioinformatics 18 (5), 747–756.
Brandstatter, M., Fromherz, P., Offenhausser, A., 1988. Fluorescent dye monolayers on oxidized silicon. Thin Solid Films 160 (1–2), 341–346.
Braun, D., Fromherz, P., 1997. Fluorescence interference-contrast microscopy of cell adhesion on oxidized silicon. Appl. Phys. A: Mater. Sci. Process. 65 (4–5), 341–348.
Chung, M., Lowe, R.D., Chan, Y.H.M., Ganesan, P.V., Boxer, S.G., 2009. DNA-tethered membranes formed by giant vesicle rupture. J. Struct. Biol. 168 (1), 190–199.
Conzone, S.D., Redkar, R.J., 2004. Reproducible, Low Cost Arraying Achieved With a Multiplexed Approach. EBR - European Biopharmaceutical Review(SPRING), pp. 52–55.
Crane, J.M., Kiessling, V., Tamm, L.K., 2005. Measuring lipid asymmetry in planar supported bilayers by fluorescence interference contrast microscopy. Langmuir 21 (4), 1377–1388.
Dabkowska, A.P., Piret, G., Niman, C.S., Lard, M., Linke, H., Nylander, T., Prinz, C.N., 2015. Surface nanostructures for fluorescence probing of supported lipid bilayers on reflective substrates. Nanoscale 7 (43), 18020–18024.
Dawson, E.D., Reppert, A.E., Rowlen, K.L., Kuck, L.R., 2005. Spotting optimization for oligo microarrays on aldehyde-glass. Anal. Biochem. 341 (2), 352–360.
Deegan, R.D., Bakajin, O., Dupont, T.F., Huber, G., Nagel, S.R., Witten, T.A., 1997. Capillary flow as the cause of ring stains from dried liquid drops. Nature 389 (6653), 827–829.
Diehl, F., Grahlmann, S., Beier, M., Hoheisel, J.D., 2001. Manufacturing DNA microarrays of high spot homogeneity and reduced background signal. Nucleic Acids Res 29 (7) (38e-38e).
Dufva, M., 2005. Fabrication of high quality microarrays. Biomol. Eng. 22 (5–6), 173–184.
Dugas, V., Broutin, J., Souteyrand, E., 2005. Droplet evaporation study applied to DNA chip manufacturing. Langmuir 21 (20), 9130–9136.
Dumont, E.L.P., Belmas, H., Hess, H., 2013. Observing the mushroom-to-brush transition for kinesin proteins. Langmuir 29 (49), 15142–15145.
Fernandez, A., 2009a. Structures for Enhanced Detection of Fluorescence. Complete Genomics, Inc., USA.
Fernandez, A., 2009b. Structures for enhanced detection of fluorescence. In: USPTO (Ed.), Official Gazette of the United States Patent and Trademark Office. Complete Genomics, Inc., USA.
Ganesan, P.V., Boxer, S.G., 2009. A membrane interferometer. Proc. Natl. Acad. Sci. USA 106 (14), 5627–5632.
Gleixner, R., Fromherz, P., 2006. The extracellular electrical resistivity in cell adhesion. Biophys. J. 90 (7), 2600–2611.
Hu, H., Larson, R.G., 2006. Marangoni effect reverses coffee-ring depositions. J. Phys. Chem. B 110 (14), 7090–7094.
Huen, T., 1979. Reflectance of thinly oxidized silicon at normal incidence. Appl. Opt. 18 (12), 1927–1932.
Iwanaga, Y., Braun, D., Fromherz, P., 2001. No correlation of focal contacts and close adhesion by comparing GFP-vinculin and fluorescence interference of DiI. Eur. Biophys. J. 30 (1), 17–26.
Jain, A.N., 2002. Fully automatic quantification of microarray image data. Genome Res. 12 (2), 325–332.
Kaizuka, Y., Groves, J.T., 2006. Hydrodynamic damping of membrane thermal fluctuations near surfaces imaged by fluorescence interference microscopy. Phys. Rev. Lett. 96, 11.
Kašpar, O., Zhang, H., Tokárová, V., Boysen, R.I., Suñé, G.R., Borrise, X., Perez-Murano, F., Hearn, M.T.W., Nicolau, D.V., 2016. Confinement of water droplets on rectangular micro/nano-arrayed surfaces. Lab a Chip 16 (13), 2487–2493.
Kerssemakers, J., Howard, J., Hess, H., Diez, S., 2006. The distance that kinesin-1 holds its cargo from the microtubule surface measured by fluorescence interference contrast microscopy. Proc. Natl. Acad. Sci. USA 103 (43), 15812–15817.
Kerssemakers, J., Ionov, L., Queitsch, U., Luna, S., Hess, H., Diez, S., 2009. 3D nanometer tracking of motile microtubules on reflective surfaces. Small 5 (15), 1732–1737.
Kiessling, V., Müller, B., Fromherz, P., 2000. Extracellular resistance in cell adhesion measured with a transistor probe. Langmuir 16 (7), 3517–3521.
Lambacher, A., Fromherz, P., 1996. Fluorescence interference-contrast microscopy on oxidized silicon using a monomolecular dye layer. Appl. Phys. a-Mater. 63 (3), 207–216.
Lambacher, A., Fromherz, P., 2002. Luminescence of dye molecules on oxidized silicon and fluorescence interference contrast microscopy of biomembranes. J. Opt. Soc. Am. B: Opt. Phys. 19 (6), 1435–1453.
Lehmussola, A., Ruusuvuori, P., Yli-Harja, O., 2006. Evaluating the performance of microarray segmentation algorithms. Bioinformatics 22 (23), 2910–2917.
Levinson, H.J., 2005. Confronting the diffraction limit. Principles of Lithography, 2nd ed. SPIE Press, Bellingham, WA, pp. 423 (pp. xii).
Marino, V., Galati, C., Arnone, C., 2008. Optimization of fluorescence enhancement for silicon-based microarrays. J. Biomed. Opt. 13, 5.
McHale, G., 2007. Surface free energy and microarray deposition technology. Analyst 132 (3), 192–195.
McQuain, M.K., Seale, K., Peek, J., Levy, S., Haselton, F.R., 2003. Effects of relative humidity and buffer additives on the contact printing of microarrays by quill pins. Anal. Biochem 320 (2), 281–291.
Moran-Mirabal, J.M., Tan, C.P., Orth, R.N., Williams, E.O., Craighead, H.G., Lin, D.M., 2007. Controlling microarray spot morphology with polymer liftoff arrays. Anal. Chem. 79 (3), 1109–1114.
Müller, U.R., Nicolau, D.V. (Eds.), 2005. Microarray Technology and Its Applications. Springer Berlin Heidelberg.
Nakache, M., Schreiber, A.B., Gaub, H., Mcconnell, H.M., 1985. Heterogeneity of membrane phospholipid mobility in endothelial-cells depends on cell substrate. Nature 317 (6032), 75–77.
Nitzsche, B., Dudek, E., Hajdo, L., Kasprzak, A.A., Vilfan, A., Diez, S., 2016. Working stroke of the kinesin-14, ncd, comprises two substeps of different direction. Proc. Natl. Acad. Sci. USA 113 (43), E6582–E6589.
Parthasarathy, R., Groves, J.T., 2004a. Optical techniques for imaging membrane topography. Cell Biochem Biophys. 41 (3), 391–414.
Parthasarathy, R., Groves, J.T., 2004b. Protein patterns at lipid bilayer junctions. Proc. Natl. Acad. Sci. USA 101 (35), 12798–12803.
Persson, M., Albet-Torres, N., Ionov, L., Sundberg, M., Höök, F., Diez, S., Månsson, A., Balaz, M., 2010. Heavy meromyosin molecules extending more than 50 nm above adsorbing electronegative surfaces. Langmuir 26 (12), 9927–9936.
Redkar, R.J., Schultz, N., Scheumann, V., Burzio, L.A., Haines, D.E., Metwalli, E., Becker, O., Conzone, S.D., 2006. Signal and sensitivity enhancement through optical interference coating for DNA and protein microarray applications. J. Biomol. Technol. 17, 2.
Rickman, D.S., Herbert, C.J., Aggerbeck, L.P., 2003. Optimizing spotting solutions for increased reproducibility of cDNA microarrays. Nucleic Acids Res 31, 18.
Rueda, L., Rezaeian, I., 2011. A fully automatic gridding method for cDNA microarray images. BMC Bioinforma. 12.
Schena, M., 2003. Microarray manufacturing. In: Schena, M. (Ed.), Microarray Analysis.

Wiley-Liss, Hoboken, NJ, pp. 163–164 (pp.).
Schuchhardt, J., 2000. Normalization strategies for cDNA microarrays. Nucleic Acids Res 28 (10) (47e-47e).
Schultz, N., Conzone, S.D., Becker, O., Haines, D., Pawlowski, E., Scheumann, V., 2011. In: USPTO (Ed.), Arrangement for Fluorescence Amplification. Official Gazette of the United States Patent and Trademark Office, Schott AG, USA.
Sorribas, H., Braun, D., Leder, L., Sonderegger, P., Tiefenauer, L., 2001. Adhesion proteins for a tight neuron-electrode contact. J. Neurosci. Methods 104 (2), 133–141.
Taylor, S., Smith, S., Windle, B., Guiseppi-Elie, A., 2003. Impact of surface chemistry and blocking strategies on DNA microarrays. Nucleic Acids Res. 31 (16) (87e-87e).
Wu, D., Song, L.B., Chen, K., Liu, F., 2012. Modelling and hydrostatic analysis of contact printing microarrays by quill pins. Int. J. Mech. Sci. 54 (1), 206–212.
Wu, W., Wildsmith, S.E., Winkley, A.J., Yallop, R., Elcock, F.J., Bugelski, P.J., 2001. Chemometric strategies for normalisation of gene expression data obtained from cDNA microarrays. Anal. Chim. Acta 446 (1–2), 451–466.
Wu, W.F., Chiou, B.S., 1996a. Optical and mechanical properties of reactively sputtered silicon dioxide films. Semicond. Sci. Technol. 11 (9), 1317–1321.
Wu, W.F., Chiou, B.S., 1996b. Properties of radio frequency magnetron sputtered silicon dioxide films. Appl. Surf. Sci. 99 (3), 237–243.
Yu, A.Y.C., Spicer, W.E., Hass, G., 1968. Optical properties of platinum. Phys. Rev. 171 (3), 834 (&).
Zeck, G., Fromherz, P., 2003. Repulsion and attraction by extracellular matrix protein in cell adhesion studied with nerve cells and lipid vesicles on silicon chips. Langmuir 19 (5), 1580–1585.